NASA TECHNICAL NOTE

NASA TN D-6633

NASA TN D-6633

ANALYSIS AND COMPARISON OF WALL COOLING SCHEMES FOR ADVANCED GAS TURBINE APPLICATIONS

by Raymond S. Colladay

Lewis Research Center
Cleveland, Ohio 44135

NATIONAL AERONAUTICS AND SPACE ADMINISTRATION • WASHINGTON, D. C. • JANUARY 1972

1. Report No.	2. Government Accession No.	3. Recipient's Catalog No.
NASA TN D-6633		

4. Title and Subtitle	5. Report Date
ANALYSIS AND COMPARISON OF WALL COOLING SCHEMES FOR ADVANCED GAS TURBINE APPLICATIONS	January 1972
	6. Performing Organization Code

7. Author(s)	8. Performing Organization Report No.
Raymond S. Colladay	E-6439
	10. Work Unit No. 764-74

9. Performing Organization Name and Address	11. Contract or Grant No.
Lewis Research Center National Aeronautics and Space Administration Cleveland, Ohio 44135	
	13. Type of Report and Period Covered
12. Sponsoring Agency Name and Address	Technical Note
National Aeronautics and Space Administration Washington, D. C. 20546	14. Sponsoring Agency Code

15. Supplementary Notes

16. Abstract

The relative performance of (1) counterflow film cooling, (2) parallel-flow film cooling, (3) convection cooling, (4) adiabatic film cooling, (5) transpiration cooling, and (6) full-coverage film cooling was investigated for heat loading conditions expected in future gas turbine engines. Assumed in the analysis were hot-gas conditions of 2200 K (3500° F) recovery temperature, 5 to 40 atmospheres total pressure, and 0.6 gas Mach number and a cooling air supply temperature of 811 K (1000° F). The first three cooling methods involve film cooling from slots. Counterflow and parallel flow describe the direction of convection cooling air along the inside surface of the wall relative to the main gas flow direction. The importance of utilizing the heat sink available in the coolant for convection cooling prior to film injection is illustrated.

17. Key Words (Suggested by Author(s))	18. Distribution Statement
Film cooling Transpiration cooling Gas turbine cooling	Unclassified - unlimited

19. Security Classif. (of this report)	20. Security Classif. (of this page)	21. No. of Pages	22. Price*
Unclassified	Unclassified	42	$3.00

* For sale by the National Technical Information Service, Springfield, Virginia 22151

ANALYSIS AND COMPARISON OF WALL COOLING SCHEMES FOR ADVANCED GAS TURBINE APPLICATIONS

by Raymond S. Colladay

Lewis Research Center

SUMMARY

Comparisons were made of six schemes for air cooling walls of gas turbine engine components. The interaction of film and convection cooling and its effect on the relative performance of the various cooling methods was investigated for an expected heat-flux range that will be encountered in future gas turbine applications. The six schemes analyzed were (1) counterflow film cooling, (2) parallel-flow film cooling, (3) convection cooling, (4) adiabatic film cooling, (5) transpiration cooling, and (6) full-coverage film cooling. The first three methods involve film cooling from slots. Counterflow and parallel flow describe the direction of convection cooling air along the inside surface of the wall relative to the main gas and film layer flow direction.

Hot-gas conditions of 2200 K (3500° F) recovery temperature; 5, 10, 20, and 40 atmospheres total pressure; and 0.6 gas Mach number were assumed. The supply cooling air temperature was assumed to be 811 K (1000° F).

The coolant required to maintain a given average wall temperature is reduced by using the heat sink available in the cooling air for convection cooling before it is ejected as a film. The most efficient use of cooling air is achieved when film and convection cooling are combined, as in transpiration, full-coverage, counterflow, and parallel-flow film cooling. The coolant requirements for counterflow film cooling are greater than for transpiration cooling, as expected, but can be less than for full-coverage film cooling. This relative order in cooling efficiency is due primarily to the respective magnitudes of the film effectiveness associated with each cooling scheme.

Low surface-temperature variations are possible with transpiration and full-coverage film cooling because of the ability to locally control mass ejection with these schemes. Counterflow film cooling yields much smaller surface-temperature variations than parallel-flow film cooling due to the complimentary interaction of film and convection cooling achieved with the counterflow arrangement.

INTRODUCTION

A number of schemes for air cooling walls of gas turbine engine components by film and convection cooling were analyzed and compared. The importance of utilizing the heat sink available in the coolant for convection cooling prior to film injection was investigated.

As indicated in reference 1, the high gas temperatures and pressures expected in future gas turbine engines make convection cooling of engine components very difficult and, in some instances, impossible even for the most effective configurations. Hence, convection cooling must be augmented by film cooling, where the film layer protects the surface from the hot gas and reduces the heat flux to the wall.

Transpiration and full-coverage film cooling schemes effectively utilizing cooling air by combining film and convection cooling. These two schemes are compared with convection cooling in reference 1. Due to the small internal coolant flow passages of a transpiration-cooled porous wall, oxidation at high wall temperatures could lead to flow blockage (ref. 2). Because of the uncertainties resulting from oxidation it is necessary to continue investigations of alternate, but effective, means of cooling under high heat-flux conditions.

In the full-coverage film cooling scheme, cooling air issues from a large number of small discrete holes in the surface. This scheme lies in the spectrum between pure transpiration cooling on the one end, with essentially a continuous mass flux over the surface, and localized film cooling on the other end. The amount of heat transferred to the cooling air flowing through the wall depends on the tortuosity of the internal flow passages. The wall may be constructed of simple, straight-through holes with a low resultant convection effectiveness; or it may consist of a maze of interconnected flow passages with a relatively high convection effectiveness. These internal passages are, in general, much larger than the pores associated with transpiration cooling; so oxidation does not present a severe problem.

The film protection provided by injection through discrete holes is much less than that available with continuous slot injection, as illustrated in reference 3. Numerous investigations have been made to study film cooling from a slot at various injection angles to the wall surface. In applications which structurally permit its use, this injection geometry can be very effective.

In this report, six schemes for cooling gas turbine engine components (e.g., plug nozzle, combustor liner, shroud, or turbine vanes and blades) were analyzed and compared assuming hot gas conditions of 2200 K (3500° F) recovery temperature; total pressures of 5, 10, 20, and 40 atmospheres; and a constant gas Mach number of 0.6. A cooling supply temperature of 811 K (1000° F) was also assumed. The six schemes are (1) counterflow film cooling, (2) parallel-flow film cooling, (3) convection cooling, (4) adiabatic film cooling, (5) transpiration cooling, and (6) full-coverage film cooling. The

first three cooling methods involve film cooling from slots. Counterflow and parallel flow describe the direction of convection cooling air along the inside surface of the wall relative to the main gas flow direction. Adiabatic film cooling assumes no convection cooling prior to the coolant being ejected as a film over the surface.

HEAT-TRANSFER MODELS

Figure 1 illustrates the heat-transfer models for six cooling schemes that were used in the analysis to show the comparative performance of convection and film cooling alone and also of combining these two modes of heat transfer. The six schemes consisted of (1) counterflow film cooling (CFFC), (2) parallel-flow film cooling (PFFC), (3) convection cooling (CONV), (4) adiabatic film cooling (ADFC), (5) transpiration cooling (TRANS), and (6) full-coverage film cooling (FCFC). The different schemes were compared on the basis of their performance in cooling a given area of length L located a distance x_o from the apparent origin of a turbulent hydrodynamic and thermal boundary layer on a flat plate. The local heat-transfer coefficient distribution in the absence of film cooling was, therefore, the same for each model.

Figure 1(a) illustrates the counterflow film cooling (CFFC) model. The coolant flows through a finned convection passage in a direction opposite to the gas stream; so the convection cooling air is at its lowest temperature in the region where the film layer has decayed the most. The cooling air is ejected from a slot inclined at 30° to the surface.

The direction of the coolant flow is reversed for parallel-flow film cooling (PFFC), as illustrated in figure 1(b). It was assumed that the temperature $T_{c,2}$ and flow rate of the cooling air leaving the slot at $x = 0$ were equal, respectively, to the temperature and flow rate of the coolant from the $x = L$ slot. This assumption maintains an overall energy balance for a given segment from $x = 0$ to $x = L$. As in the CFFC case, fins were assumed in the cooling passage.

The convection cooling (CONV) model illustrated in figure 1(c) is identical to the PFFC model except that the cooling air is never used for film cooling.

In each of the cooling models - CFFC, PFFC, and CONV - the containing wall forming the bottom of the convection passage was considered to be a structural member insulated on the coolant plenum surface and was assumed to be passive from a heat-transfer standpoint. As a reference case for the majority of the analyses for these models, the outer wall thickness t was assumed to be 0.05 centimeter (0.02 in.). The effect of varying this thickness is investigated. A coolant passage height of 0.064 centimeter (0.025 in.) was assumed.

In the adiabatic film cooling (ADFC) scheme illustrated in figure 1(d), the wall is cooled only by the film layer protecting the surface from the hot gas. The cooling air

does no convection cooling prior to leaving the slots. For comparison purposes, the wall thickness and slot injection angle were assumed to be the same as for the CFFC and PFFC cases.

The transpiration cooling (TRANS) model is illustrated in figure 1(e). With this scheme, the mass flux is essentially continuous over the surface; so the film layer is uniform. Also, large quantities of heat can be transferred to the cooling air flowing through the porous wall.

The full-coverage film cooling (FCFC) scheme is illustrated in figure 1(f). This scheme, with cooling air ejected from a large number of small discrete holes, lies in the spectrum between pure transpiration cooling and film cooling. Although only inclined holes are shown in the figure, various internal passage configurations can be considered to increase the rate of convective heat transfer to the cooling air flowing through the wall.

For the latter two cooling schemes the wall thickness was assumed to be equal to the combined thickness of the outer wall and passage height of the CFFC, PFFC, and CONV schemes, namely 0.114 centimeter (0.045 in.). Also, for these two cooling schemes it was assumed that the local coolant mass flux could be varied in proportion to the heat-flux distribution to yield a constant hot-gas-side surface temperature.

It should be noted that only the heat transferred to the wall by convection is considered in the comparison of the various cooling schemes. In a particular application, the additive heat flux due to radiation from the surrounding surfaces and from the combustion gas should be considered in evaluating total coolant requirements.

HEAT-TRANSFER ANALYSIS

Film-Convection Cooling Analysis

This section deals with the heat-transfer relations associated with film cooling from a slot in conjunction with convection cooling.

The heat transferred to a film-cooled surface from the hot gas stream can be expressed in terms of the film cooling adiabatic wall temperature T_{aw} as

$$dq_g = h_{gx}(T_{aw} - T_{w,2})dA \tag{1}$$

(All symbols are defined in the appendix.) Eliminating the local adiabatic wall temperature by introducing the film effectiveness

$$\eta_{film} = \frac{T_{ge} - T_{aw}}{T_{ge} - T_{c,2}}$$

leads to (for a unit width)

$$dq_g = h_{gx}\left(\frac{T_{ge} - T_{w,2}}{T_{ge} - T_{c,2}} - \eta_{film}\right)(T_{ge} - T_{c,2})dx \tag{2}$$

The effective gas temperature T_{ge} (or the adiabatic wall temperature without film cooling or recovery temperature) is defined as $T_{ge} = t_g + \Lambda(T_g - t_g)$ with $\Lambda = Pr^{1/3}$ for turbulent flow.

The heat transferred to the coolant from a finned surface is

$$dq_c = h_c(T_{w,1} - T_c)dA_{eff} \tag{3}$$

The heat transferred to the coolant is also given by

$$dq_c = G_{c,p}A_pC_{p,c}\,dT_c = G_cC_{p,c}L\,dT_c \tag{4}$$

for a unit width. The mass velocity G_c is the average mass-flux rate based on the total cooled surface area, that is,

$$G_c = \frac{\text{Coolant flow rate}}{\text{Total cooled surface area}}$$

The local wall temperature is computed numerically by requiring a local energy balance between film cooling, wall conduction, and convection cooling that satisfies equations (2) to (4). Wall conduction in the x-direction, as well as in the direction normal to the surface, is accounted for in the analysis.

Gas-to-surface heat-transfer coefficient. - The local heat-transfer coefficient as defined by equation (1) was assumed to be independent of blowing rate. Using the local Nusselt number correlation for a flat plate from reference 4 with a turbulent hydrodynamic and thermal boundary layer origin at $x = -x_o$,

$$Nu = \frac{h_{gx}x}{k} = 0.0296\,Re_x^{0.8}Pr^{1/3} \tag{5}$$

An x_o value of 2.5 centimeters (1 in.) was assumed in this analysis. The fluid properties in equation (5) were evaluated at the local reference temperature given in reference 5.

$$T_{ref} = 0.5\,T_{w,2} + 0.28\,t_g + 0.22\,T_{ge} \tag{6}$$

Values of thermal conductivity, Prandtl number, specific heat, and viscosity were obtained from reference 6 for the combustion products of air and ASTM-A-1 fuel at a pressure of 10 atmospheres and a fuel-air ratio of 0.06.

Combining equations (5) and (6) with Mach number, pressure, and temperature relations for a constant Prandtl number of 0.7 results in

$$h_{gx} = 0.026\,K\left[\frac{PM\sqrt{\frac{\gamma T_g}{R}}}{\mu T_{ref}\left(1 - \frac{\gamma - 1}{2}M^2\right)^{(3\gamma-1)/2(\gamma-1)}}\right]^{0.8} x^{-0.2} \tag{7}$$

Finned surface convection. - In order to transfer enough heat to the cooling air by convection, a finned cooling passage for the CFFC, PFFC, and CONV schemes was considered. Chosen for this study as an example of one of the more effective finned surfaces with possible application to turbine cooling is the offset rectangular plate fin shown schematically in figure 2. The friction and heat-transfer data for this fin configuration were obtained from reference 7. Due to the continual interruption and reattachment of the boundary layer, the heat-transfer coefficient is of the order of twice that of an ordinary rectangular plate fin. The base conditions assumed for the fin dimensions in this study were (1) passage height b, 0.064 centimeter; (2) fin thickness δ, 0.0076 centimeter (0.003 in.); (3) number of fins per centimeter NF, 16; and (4) a fin material of nickel.

In an actual design, the fin configuration would be dictated by the constraints imposed. To investigate the effect that the fin configuration has an overall cooling efficiency, the coolant-side surface conductance was varied from the offset plate fin value to zero (insulated surface) for a representative CFFC case.

The coolant-side heat-transfer coefficient used in equation (3) is expressed in terms of the Colburn factor j as a function of Reynolds number for the given fin configuration (from ref. 7)

$$h_c = G_{c,p}C_{p,c}jPr^{-2/3} \tag{8}$$

Air properties were obtained from reference 6 at 10 atmospheres.

The effective surface area in equation (3) is defined in terms of the fin effectiveness as follows

$$A_{eff} = A_{uf} + A_{fin}\,\eta_{fin} \tag{9}$$

where

$$\eta_{fin} = \frac{\tanh\left(l\sqrt{\frac{2h_c}{k\delta}}\right)}{l\sqrt{\frac{2h_c}{k\delta}}} \tag{10}$$

with

$$A_{uf} = [1 - (NF)\delta]L \tag{11}$$

$$A_{fin} = 2bL(NF) + [1 - (NF)\delta]L \tag{12}$$

$$l = b + \frac{1}{2}\left(\frac{1}{NF} - \delta\right) \tag{13}$$

for a unit width in the lateral direction.

Film effectiveness. - In this study, the local variation in film temperature downstream of the slot is required in the wall energy balance. As the relatively cool film entrains hot gas from turbulent mixing at the interface, the effectiveness of the film as an insulating barrier diminishes.

Numerous investigations have been performed to measure the film effectiveness η_{film} under a variety of conditions. The η_{film} data have been correlated against the dimensionless length x/ms, and also against such additional parameters as coolant slot Reynolds number, gas Reynolds number, specific-heat ratio, and density ratio. The film effectiveness data correlated against x/ms from reference 8 were felt to be representative for the conditions of this study.

In evaluating the coolant flow rate required to maintain the surface below a given temperature, it is more appropriate to relate the film effectiveness to the coolant flow rate per unit cooled surface area G_c than to the flow rate per unit slot area. Expressing the coolant- to gas-flow-rate ratio m in terms of G_c leads to the following expres-

sion for x/ms, which is independent of the slot height s:

$$m = \frac{(\rho V)_s}{G_g} \tag{14}$$

where for a unit width along the slot

$$(\rho V)_s = G_c \frac{L}{s}$$

Therefore,

$$\frac{x}{ms} = \frac{G_g}{G_c}\left(\frac{x}{L}\right) \tag{15}$$

Note that for given hot-gas conditions and coolant flow rate per unit surface area (fixed G_g/G_c ratio), changing the length L of the film-convection assembly does not change the surface averaged (x = 0 to x = L) film effectiveness if η_{film} is expressed solely in terms of x/ms as in the present study.

Numerical method. - The outer wall from x = 0 to x = L was divided into a number of nodes. A numerical solution of the steady-state, two-dimensional, heat-conduction equation was used to generate the wall temperature distribution satisfying an energy balance at each node. An iteration was required due to the interdependence of (1) the wall temperature distribution, (2) the coolant temperature rise through the finned passage, (3) the adiabatic wall temperature decay downstream of the slot, (4) the coolant-side heat-transfer coefficient, (5) the fin effectiveness, and (6) the hot-gas-side heat-transfer coefficient.

The flow chart in figure 3 gives a general outline of the program logic. The iteration loop shown in the left portion of the diagram is used to determine the coolant flow rate required to maintain a maximum surface temperature of 1255 K (1800° F). If the wall temperature distribution for a given coolant flow rate is needed, this loop is bypassed.

No wall conduction. - An energy balance on a counterflow or parallel-flow film-cooled wall yields a closed-form analytical expression for the average wall temperature if wall conduction is neglected. Even though conduction is important under the conditions of this study, the resulting expression is, nevertheless, useful in a qualitative sense, in providing insight into the interaction of film and convection cooling.

Equating dq_g and dq_c defined by equations (2) and (4) respectively, assuming an average hot-gas-side heat-transfer coefficient and noting that $T_{w,1} = T_{w,2} = T_w$, gives

$$\frac{G_c C_{p,c}}{\bar{h}_g} dT_c = \pm(T_{c,2} - T_{ge})\left(\frac{T_{ge} - T_w}{T_{ge} - T_{c,2}} - \eta_{film}\right) d\xi \tag{16}$$

where $\xi = x/L$, and the positive and negative signs correspond to CFFC and PFFC, respectively. Integrating from $\xi = 0$ to $\xi = 1$ and rearranging yields the following expression for the average wall temperature

$$\left(T_w\right)_{avg} = \left(\bar{\eta}_{film} - \frac{G_c C_{p,c}}{\bar{h}_g}\right) T_{c,2} + \left(1 - \bar{\eta}_{film}\right) T_{ge} + \frac{G_c C_{p,c}}{\bar{h}_g} T_{c,i} \tag{17}$$

Rearranging equation (17) yields the following expression for the coolant mass-flux parameter $G_c C_{p,c}/\bar{h}_g$ in terms of the convection effectivnesss η', defined as

$$\frac{T_{c,2} - T_{c,i}}{\left(T_{w,2}\right)_{max} - T_{c,i}}$$

$$\frac{G_c C_{p,c}}{\bar{h}_g} = \bar{\eta}_{film} + \frac{1}{\eta'}\left(\bar{\varphi} - \bar{\eta}_{film}\right)\frac{1}{1 - \varphi_{min}} \tag{18}$$

where

$$\bar{\varphi} = \frac{T_{ge} - \left(T_{w,2}\right)_{av}}{T_{ge} - T_{c,i}}$$

and

$$\bar{\varphi}_{min} = \frac{T_{ge} - \left(T_{w,2}\right)_{max}}{T_{ge} - T_{c,i}}$$

with $T_{w,2} = T_w$ for this case. Convection effectiveness is a measure of the efficiency of the configuration is transferring heat to the coolant by convection.

Summation of film effectiveness for multiple slots. - When a series of slots are considered, a residual film layer from an upstream slot affects the region downstream of subsequent slots. To obtain an upper bound for the film effectiveness, it was assumed that each slot sees the previous slots' adiabatic wall temperature.

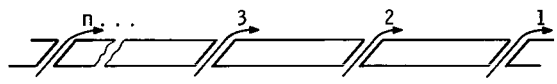

(a)

For two slots in series (see sketch (a)), the film effectiveness downstream of the second slot can be expressed as (from ref. 9)

$$\eta_{film} = \eta_1 + \eta_2(1 - \eta_1)$$

where η_1 and η_2 are the film effectiveness distributions for each respective slot considered independently.

For n slots, the film effectiveness for the slot furthest downstream becomes

$$\eta_{film} = \eta_1 + \eta_2(1 - \eta_1) + \eta_3(1 - \eta_1)(1 - \eta_2) + \ldots + \eta_n(1 - \eta_1) \ldots (1 - \eta_{n-1})$$

Transpiration and Full-Coverage Film Cooling Analyses

A high convection effectiveness and uniform film layer on the surface make transpiration cooling one of the most efficient cooling schemes for use in high-gas-temperature applications. Full-coverage film cooling, with cooling air ejected from a large number of small discrete holes in the surface, lies in the spectrum between pure transpiration and localized film cooling. The convection effectiveness for FCFC varies depending on the internal structure of the wall.

It was assumed that the coolant mass-flux rate for the TRANS and FCFC schemes could be varied in proportion to the no blowing heat-transfer-coefficient distribution along the surface in order to maintain a constant surface temperature. However, only the average coolant mass-flux rate over the surface area extending from $x = 0$ to $x = L$ is of interest for comparison with slot film cooling. The average coolant mass-flux rate G_c was calculated by using the average hot-gas-side heat-transfer coefficient $\bar{h}_g$ where

$$\bar{h}_{g,L} = \frac{1}{L} \int_{x_o}^{x_o+L} h_{g,x}\, dx$$

By integrating equation (7),

$$\bar{h}_{g,L} = 0.0325\, k_g \left[\frac{PM \sqrt{\frac{\gamma T_g}{R}}}{\mu T_{ref} \left(1 + \frac{\gamma - 1}{2} M^2\right)^{(3\gamma-1)/2(\gamma-1)}} \right]^{0.8} \frac{(L + x_o)^{0.8} - x_o^{0.8}}{L} \tag{19}$$

The heat flux to a transpiration- or full-coverage-film-cooled wall is usually expressed in terms of a reduced heat-transfer coefficient and the wall temperature, namely,

$$q = h_g \left(\frac{h}{h_g}\right)(T_{ge} - T_{w,2}) \tag{20}$$

where h equals h_{trans} or h_{fcfc}, depending on the cooling method. By expressing the heat flux in this manner, it is assumed that the effective gas temperature T_{ge} is unaffected by blowing. This heat flux can also be expressed in terms of the rise in cooling air temperature as

$$q = G_c C_{p,c}(T_{c,2} - T_{c,i})$$

or in terms of the internal convection effectiveness

$$q = G_c C_{p,c} \eta'(T_{w,2} - T_{c,i}) \tag{21}$$

where η' can be for either TRANS or FCFC.

The reduction in gas-to-wall heat-transfer coefficient for transpiration cooling has been determined experimentally in references 10 to 14 for $\eta'_{trans} = 1$, and the results agree with the following relation developed in references 15 and 16:

$$\frac{h_{trans}}{h_g} = \frac{B}{e^B - 1} \tag{22}$$

where

$$B = \frac{G_c C_{p,c}}{h_g} \frac{C_{p,g}}{C_{p,c}}$$

The performance of a full-coverage film-cooled-type wall with a large number of discretely spaced coolant ejection holes is not as well defined. One such wall has been studied in detail for a turbine cooling application and reported in reference 17. The wall is composed of laminates of perforated sheet metal with injection hole diameters typically 0.04 to 0.05 centimeter (0.016 to 0.020 in.) and spaced at 3 to 7 diameters in a staggered array. The following empirical relation (from ref. 18) correlates heat-transfer data for a number of these laminated FCFC walls when the convection effectiveness is approximately 0.7:

$$1 - \varphi = \left[1 + 0.34\left(\frac{G_c C_{p,c}}{h_g}\right)\right]^{-2.28} \tag{23}$$

where

$$\varphi = \frac{T_{ge} - T_{w,2}}{T_{ge} - T_{c,i}}$$

Equating the heat-flux expressions in equations (20) and (21) and solving for the h/h_g ratio for FCFC yields

$$\frac{h_{fcfc}}{h_g} = \frac{1 - \varphi}{\varphi} \eta'_{fcfc} \frac{G_c C_{p,c}}{h_g} \tag{24}$$

Substituting equation (23) into equation (24) with $\eta'_{fcfc} = 0.7$ yields the desired reduction in the heat-transfer coefficient.

In both the TRANS and FCFC cases, the heat-transfer-coefficient ratio is known only at the specified values of η'. It would be desirable to extend the analysis of TRANS and FCFC to η' values other than the reference values of 1.0 and 0.7, respectively.

Transpiration-cooled walls in gas turbine engines will be thin (about 0.08 to 0.13 cm) with a limited amount of internal surface area in contact with the coolant, so η'_{trans} will likely be less than 1.0. Also, the value of η'_{fcfc} can vary significantly depending on the extent that the back side (coolant side) of the perforated plate is augmented to allow greater surface area for increased convective heat transfer.

The following method was used for extrapolation of h/h_g to lower values of convection effectiveness: The heat flux to a transpiration-cooled or full-coverage-film-cooled wall can also be defined in terms of a film cooling effectiveness and h_g. In the FCFC case with discrete coolant ejection holes, η_{film} varies locally around each hole. References 3, 19, and 20 investigate the film-cooling effectiveness for one ejection hole or a row of ejection holes. However, since only the average outer wall temperature $T_{w,2}$ is desired, an average film effectiveness over a surface area sufficiently large to contain a group of holes is considered.

Let $\bar{\eta}_{film}$ be the average film effectiveness over the surface of length L in the gas flow direction, then

$$q = \bar{h}_g\left(\bar{T}_{aw} - T_{w,2}\right) = \bar{h}_g\left(\frac{T_{ge} - T_{w,2}}{T_{ge} - T_{c,2}} - \bar{\eta}_{film}\right)(T_{ge} - T_{c,2}) \tag{25}$$

Equating the heat flux given by equation (20) averaged over the surface with that given by equation (25), expressing $T_{c,2}$ in terms of the convective effectiveness and φ, and rearranging yields

$$\bar{\eta}_{film} = \frac{\varphi\left(1 - \dfrac{\bar{h}}{\bar{h}_g}\right)}{1 + \eta'_o(\varphi - 1)} \tag{26}$$

where η'_o is the reference value of the convection effectiveness at which the $\bar{h}/\bar{h}_g$ ratio is known.

It was assumed that $\bar{\eta}_{film}$ is independent of η' for a given coolant ejection surface. This assumption is reasonable if the effect of density ratio (coolant to gas) on $\bar{\eta}_{film}$ is accounted for entirely through the mass-flux ratio. Equation (26) then gives

$$\bar{\eta}_{film} = f\left(\frac{G_c C_{p,c}}{\bar{h}_g}\right)$$

for TRANS and FCFC when the $\bar{h}/\bar{h}_g$ ratio is substituted from equations (22) and (24), respectively, with $\eta'_{o,trans} = 1$ and $\eta'_{o,fcfc} = 0.7$.

Finally, to obtain the functional relation between the coolant flow rate and η', the heat-flux expressions given by equations (21) and (25) were equated, yielding

$$\frac{G_c C_{p,c}}{\bar{h}_g} = \bar{\eta}_{film} + \frac{1}{\eta'}\left(\varphi - \bar{\eta}_{film}\right)\frac{1}{1-\varphi} \tag{27}$$

with $\bar{\eta}_{film}$ given by equation (26).

The convection effectiveness in equation (27) is not constant but rather decreases as G_c increases. In order to determine the functional dependence of η' on G_c, the porous wall model from reference 21 was used with an internal volumetric heat-transfer coefficient H_m taken from reference 22. The coefficient H_m is the product of the internal-porous-surface-to-coolant heat-transfer coefficient and the internal surface area per unit volume. As indicated in reference 22, H_m is proportional to G_c for the majority of porous wall materials investigated. Typical distributions of η'_{trans} and η'_{fcfc} used in this study are given in figure 4 assuming an effective wall thermal conductivity of 13.8 J/(sec)(m)(K) (8 Btu/(hr)(ft)(^{o}F) and a wall thickness of 0.114 centimeter.

Note that equations (27) and (18) are of the same form. The parameters φ, $\bar{\varphi}$, and φ_{min} are all equal for TRANS and FCFC by assumption that a constant wall temperature could be maintained. By rearranging equation (27), the outer wall temperature can be expressed as

$$T_{w,2} = \left(\bar{\eta}_{film} - \frac{G_c C_{p,c}}{\bar{h}_g}\right)T_{c,2} + \left(1 - \bar{\eta}_{film}\right)T_{ge} + \frac{G_c C_{p,c}}{\bar{h}_g}T_{c,i} \tag{28}$$

This is the same form as equation (17).

PRESSURE DROP ANALYSIS

In an actual design, the most effective heat-transfer surface would be chosen to comply with the coolant supply pressure available. In this study, the pressure required to maintain a given coolant flow rate is simply stated as a result of the particular configuration, with the understanding that for certain applications some configurations would be impossible.

Due to the expected superiority of CFFC over PFFC and CONV and to the similar

flow configuration for these three schemes, the pressure drop analysis was limited to the CFFC scheme. For the TRANS and FCFC schemes, the pressure drop depends on the porosity and internal matrix structure of the wall, which have not been specified for this study.

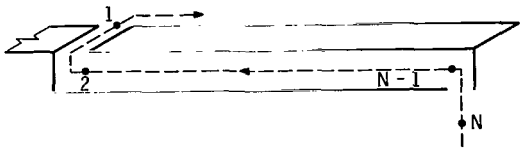

(b)

Referring to sketch (b), the total-pressure drop around the exit bend can be expressed in terms of the momentum flux at station 2:

$$P_{(2)} - P_{(1)} = K'' \frac{G_{c,p}^2}{2\rho_{(2)}} \tag{29}$$

Introducing relations among parameters M, P, T, and ρ from reference 23 leads to the following expressions for pressure and Mach number:

$$p_{(2)} = \frac{p_{(1)}\left[1 + \frac{\gamma - 1}{2} M_{(1)}^2\right]^{\gamma/\gamma-1}}{\left[1 + \frac{\gamma - 1}{2} M_{(2)}^2\right]^{\gamma/\gamma-1} - \frac{1}{2} K''\gamma M_{(2)}^2} \tag{30}$$

$$P_{(2)} = p_{(2)}\left[1 + \frac{\gamma - 1}{2} M_{(2)}^2\right]^{\gamma/\gamma-1} \tag{31}$$

$$M_{(i)} = \left[\sqrt{\frac{1}{(\gamma - 1)^2} + \frac{2}{\gamma - 1} \frac{G_{c,p}^2 RT_{(i)}}{p_{(i)}^2 \gamma}} - \frac{1}{\gamma - 1}\right]^{1/2} \qquad i = 1, 2 \tag{32}$$

with $K'' = 1.0$, and $p_{(1)}$ known from free-stream gas conditions. Conditions at station 2 were calculated by iterating between equations (30) and (32).

The variation in Mach number along the heated length due to pressure drop caused by friction and momentum change can be expressed by the following differential equation (ref. 20):

$$dM = \frac{1}{2}\frac{(1+\gamma M^2)M\left(1+\frac{\gamma-1}{2}M^2\right)}{1-M^2}\frac{1}{T_c}dT_c + \frac{1}{2}\frac{\gamma M^3\left(1+\frac{\gamma-1}{2}M^2\right)}{1-M^2}\frac{4f_{opf}}{D_H}dL \tag{33}$$

Equation (33) was integrated numerically to yield Mach number as a function of x.

The static pressure at any node i between $x = 0$ and $x = L$ can then be expressed by

$$\frac{p_{(i)}}{p_{(i-1)}} = \left[\frac{M_{(i-1)}}{M_{(i)}}\right]\left\{\frac{T_{(i)}\left[1+\frac{\gamma-1}{2}M^2_{(i-1)}\right]}{T_{(i-1)}\left[1+\frac{\gamma-1}{2}M^2_{(i)}\right]}\right\}^{1/2} \qquad i = 3, 4, \ldots, N-1 \tag{34}$$

The total-pressure drop in going from the plenum at station N, through a contraction, and around a bend to station $N - 1$ is expressed in terms of the kinetic energy at station $N - 1$:

$$P_{(N)} - P_{(N-1)} = K'\frac{G^2_{c,p}}{2\rho_{(N-1)}} \tag{35}$$

$$p_{(N)} = P_{(N)} = P_{(N-1)} + \frac{K'G^2_{c,p}RT_{(N-1)}}{2P_{(N-1)}\left[1+\frac{\gamma-1}{2}M^2_{(N-1)}\right]^{1/1-\gamma}} \tag{36}$$

The ratio of the pressure required in the plenum to force a given coolant flow through the configuration to the exit pressure is presented in terms of $p_{(N)}/p_{(1)}$.

RESULTS AND DISCUSSION

In this section, six schemes for cooling walls of gas turbine engine components are compared. The interaction of film and convection cooling and its effect on the relative performance of the various cooling methods is also discussed. The six schemes are (1) counterflow film cooling (CFFC), (2) parallel-flow film cooling (PFFC), (3) convection cooling (CONV), (4) adiabatic film cooling (ADFC), (5) transpiration cooling (TRANS), and (6) full-coverage film cooling (FCFC). Hot-gas conditions of 2200 K (3500° F) recovery temperature; 5, 10, 20, and 40 atmospheres total pressure; and an average gas-channel Mach number of 0.6 were assumed. Furthermore, a coolant supply temperature of 811 K (1000° F) was assumed. A detailed comparison of FCFC, TRANS, and CONV cooling was made in reference 1. Of the remaining three schemes, CFFC is given more emphasis in this report, based on its expected superior performance over the PFFC and ADFC schemes.

Interaction of Convection and Film Cooling

Using cooling air for convection cooling prior to its being injected as a film raises the exit coolant temperature $T_{c,2}$ and therefore increases the heat flux to the wall because of the resulting higher adiabatic wall temperature. The interaction of the two modes of heat transfer in series is most clearly demonstrated by the energy balance relations developed in the section entitled HEAT-TRANSFER ANALYSIS; namely, equations (17) and (18) for CFFC and equations (27) and (28) for TRANS and FCFC. Recall that equations (17) and (18) should be interpreted only qualitatively since wall conduction was neglected in order to obtain explicit algebraic expressions for the average wall temperature and coolant flow rate. All the specific results which follow account for conduction in the wall.

If the coefficient of $T_{c,2}$ in equations (17) and (28) is negative, the average wall temperature would be expected to decrease for a given coolant flow rate and given hot-gas conditions because of the increase in convective heat-transfer rate to the coolant (causing an increase in $T_{c,2}$) before it is ejected as a film. The temperature gradients in the CFFC case may, however, increase as a result.

Figure 5 indicates that for the conditions of this study, the dimensionless group $G_c C_{p,c}/\bar{h}_g$ is always greater than $\bar{\eta}_{film}$; hence, the coefficient of $T_{c,2}$ in equations (17) and (28) is negative. The value of G_c in figure 5 is the coolant flow rate per unit cooled surface area required to maintain a 1255 K (1800° F) constant surface temperature for TRANS and FCFC or, in the case of CFFC, to maintain a 1255 K (1800° F) maximum surface temperature. The more efficient the cooling method, the lower the

$G_c C_{p,c}/h_g$ value is for a given value of $\bar{\eta}_{film}$; and since transpiration cooling is the most efficient cooling method, it represents a lower bound in $G_c C_{p,c}/h_g$ in figure 5.

Consider transpiration and full-coverage film cooling. The curves in figure 5 corresponding to these schemes are independent of pressure and length L - these variables being absorbed in the evaluation of h_g. (Recall that the results are for typical but specific wall configurations, namely a wall thickness of 0.114 cm and effective thermal conductivity equal to 13.8 J/(sec)(m)(K). The convection effectiveness follows the respective distribution given in fig. 4. The injection hole array for FCFC assumes staggered holes with hole diameter and spacing in a range of 0.04 to 0.05 cm and 3 to 7 diameters, respectively.) The independent variable in figure 5 is the convection effectiveness with the $(G_c C_{p,c}/h_g)$-against-η' curves on the left. The corresponding η_{film} curves, related to the η' curves by a common value of $G_c C_{p,c}/h_g$ appear on the right. For example, given h_g and $C_{p,c}$, a FCFC wall with a convection effectiveness of 0.6 would require a coolant mass-flux rate G_c yielding a $G_c C_{p,c}/h_g$ value of 2.05 for wall and coolant supply temperatures of 1255 and 811 K, respectively. Reading across to the η_{film} curve at the given value of $G_c C_{p,c}/h_g$, the corresponding film effectiveness is 0.35. If the convection effectiveness is reduced, the coolant mass-flux rate must increase to maintain the required surface temperature. The increased coolant mass flux simultaneously increases the film effectiveness, which reduces the sensitivity of G_c to η' from what would otherwise exist in the absence of film cooling.

A simple perforated FCFC wall which has an η'_{fcfc} value of about 0.2 (typical of a wall with straight holes and plenum-supplied cooling air) would require approximately 60 percent more cooling air than a wall having the same injection hole array but with a convection effectiveness of 0.6.

For comparison, $(G_c C_{p,c}/h_g)$-against-$\bar{\eta}_{film}$ curve for the CFFC configuration is included in figure 5 for a restricted range of conditions, namely gas pressures from 5 to 40 atmospheres and values of I (axial length of the counterflow segment) from 2.5 to 25 centimeters. The corresponding range in η'_{cffc} is from 0.32 to 0.95. The reason for the spread of the CFFC results is that although $(T_{w,2})_{max}$ is maintained at 1255 K (1800° F), the average wall temperature varies considerably with pressure and length L. For the given range of conditions represented by this shaded area, η' for TRANS and FCFC range from 0.67 to 0.82 and from 0.45 to 0.63, respectively.

By increasing η', the temperature of the film layer acting as a buffer between the wall and the hot gas increases, causing an increase in the heat flux to the wall. However, even though the film layer is at a higher temperature, the gain from increasing convection to the coolant upstream of the film injection point dominates the overall energy balance and results in a reduction of coolant flow necessary to maintain a given wall temperature. As the difference between the hot gas and wall temperature decreases, this

result becomes less apparent, as indicated for FCFC in figure 6, where two additional gas temperatures (1645 and 2480 K, or 2500° and 4000° F) have been included.

Counterflow Film Cooling

The CFFC scheme was investigated in detail for an effective fin geometry, namely, the offset plate fin described in the section entitled HEAT-TRANSFER ANALYSIS. The effect of reducing the heat-transfer efficiency of the finned surface is also discussed.

The response of a wall section cooled by this CFFC configuration subjected to hot-gas conditions of 2200 K (3500° F) recovery temperature and pressures of 5, 10, 20, and 40 atmospheres is shown in figures 7(a) to (d), respectively. Included is (1) the ratio of the coolant flow rate per total cooled surface area to the mass velocity of the hot gas (coolant mass-flux ratio G_c/G_g) required to maintain the maximum surface temperature at 1255 K (1800° F), (2) the pressure ratio $p_{(N)}/p_{(1)}$ required to force that coolant through the configuration, and (3) the resulting surface-temperature distribution from $x = 0$ to $x = L$. The length L of the counterflow section was varied from 2.5 to 25 centimeters. A large variation in length L was covered to include a number of possible cooling applications in high-temperature gas turbine engines such as turbine blades and vanes, combustor liners, plug nozzles, and shrouds, and to demonstrate the effect of increasing L.

Relative coolant flow rate requirements. - For a fixed value of coolant mass-flux rate G_c, increasing the length L increases the flow rate through the cooling passage (and consequently increases the heat transferred from the wall by convection) while the film effectiveness averaged over the surface from $x = 0$ to $x = L$ remains unchanged. Under these conditions, the wall temperature must decrease. If, as is the case in figure 7, the maximum wall temperature is maintained constant, the coolant mass-flux rate G_c decreases as L increases. Note, however, that the flow rate through the finned passages still increases with L. The average film effectiveness over the surface decreases with the reduction in G_c, but the increase in convection effectiveness η' with L dominates in the overall energy balance described qualitatively by equation (18). That η' increases with L can be seen in figure 8 where convection effectiveness is given as a function of L for gas pressures of 5, 10, 20, and 40 atmospheres. The coolant flow rate through the passage $G_{c,p}A_p$ increases with increasing pressure more rapidly than does the heat flux to the wall due to the increase in density and decrease in coolant-side wall temperature $T_{w,1}$. Consequently, the convection effectiveness decreases with increasing pressure, as illustrated in figure 8.

One factor to keep in mind when interpreting these results is that as the section length L increases and the coolant flow rate from the slot increases, the film effectiveness does not decrease as the blowing rate (ρV ratio, m) becomes large. Hence, there

is no loss in film protection in going to the longer counterflow sections with a constant flow rate per unit area, G_c. This is not the case for film injection through a row of holes where the film effectiveness decreases when an optimum blowing rate is exceeded.

Pressure requirements. - The pressure ratio in figure 7 is the ratio of the plenum pressure required to force the given coolant through the assembly to the static pressure of the gas stream. Since the pressure drop is proportional to the square of the mass velocity within the cooling passage, the required plenum pressure increases substantially with L. In designing for a particular application, the available pressure drop limits the length of the counterflow-film-cooled section.

Surface-temperature distribution. - The temperature profiles in figure 7 exhibit a maximum at a point between the convection passage inlet and the film slot due to the interaction between film and convection cooling with the counterflow configuration. In the region to the left of the maximum, film cooling plays the major role; and to the right, convection cooling dominates.

As the length of the section increases, the temperature near the slot increases and the temperature at $x = L$ decreases due to the increase in η' with L. The opposite trend occurs for a given value of L as the gas pressure increases; namely, η' decreases, causing the temperature at the slot end of the section to decrease and the temperature at $x = L$ to increase. These results are demonstrated more clearly in figure 9, where the section end-point temperatures from figure 8 are plotted as a function of L for each of the total gas pressures. The difference between the $(T_{w,2})_{max}$ line and the solid portion of the surface-temperature curves represents the maximum temperature difference for any value of L. The surface-temperature gradients decrease with increasing length; but a distinct minimum in the temperature variation over the surface occurs at each pressure when the two end-point temperatures are equal - a condition in which a balance exists between film and convection cooling.

Often, large wall-temperature differences must be avoided from a thermal stress standpoint. For the short sections operating at high pressure, the exit coolant temperature $T_{c,2}$, and hence the temperature of the film layer near the slot, is low due to the low convection effectiveness. As a result, the lowest surface temperature occurs near the slot. In this case, the surface-temperature difference can be reduced either by increasing the rate of convection (which would be difficult since the offset plate fins are already very effective) or by using a greater quantity of preheated cooling air.

Effect of reducing overall coolant-side conductance. - For the long sections operating at low pressures, the convection effectiveness is high and leads to low surface temperatures at the coolant inlet end of the segment. In this case, the rate of convection near the inlet can be reduced in order to decrease the surface-temperature variation. However, if the rate of convection elsewhere in the passage is not increased, the average surface temperature would be expected to increase (see eq. (17)) for a fixed coolant flow rate. The effect of reducing the overall finned surface conductance uni-

formly over the passage length from that of the offset plate fin to zero (insulated) while maintaining a constant coolant flow rate is shown in figure 10 for an example case of 5 atmospheres total gas pressure and a section length of 7.5 centimeters (3 in.). If the conductance is decreased approximately 50 percent from the offset plate fin value, the maximum surface-temperature difference is minimized, and $(T_{w,2})_{max}$ increases 25 K.

Effect of wall thickness. - An increase in the relative coolant flow rate required to maintain the maximum surface temperature at 1255 K (1800° F) as the wall thickness increases is shown in figure 11 for a representative case of 40 atmospheres gas pressure. The relative coolant flow rates are normalized by the corresponding values for a wall thickness of 0.05 centimeter for the three section lengths (2.5, 12.5, and 25 cm) in figure 11. A reduction of the wall thickness causes an increase in temperature of the inner surface in contact with the coolant, thereby reducing the required coolant flow rate.

Comparison of Temperature Distributions of the Various Cooling Schemes

Local surface temperature between $x = 0$ and $x = L$ are given in figure 12 for each of the six cooling schemes (CFFC, PFFC, ADFC, CONV, TRANS, and FCFC) for gas pressures of 5 and 40 atmospheres. Also, parameters η', η_{film}, φ, and φ_{min} are given in an insert table on each of the figures 12(a) to (d). All the cooling schemes at a given pressure are compared at the same cooling-air flow rate, namely, that which yields a maximum surface temperature for CFFC of 1255 K (1800° F). At each pressure, the cooling methods are all applied to the same surface area of axial length L located in the same position x_0 relative to the apparent origin of the turbulent hydrodynamic and thermal boundary layer.

The finned surface configuration is the same for CFFC, PFFC, and CONV. Only the coolant flow direction is reversed between CFFC and PFFC; and in the CONV case, the coolant is not injected over the surface after flowing through the finned passage. For PFFC, the film cooling air ejected from the slot is assumed to be equal in mass flow rate and temperature to the coolant exiting the finned passage.

Minimum surface-temperature variation for CFFC. - In figures 12(a) and (b), the axial length L of the cooled wall was chosen to minimize the surface-temperature variation for CFFC. From figure 9, the appropriate values of L are 3.0 and 17.7 centimeters for gas pressures to 5 and 40 atmospheres, respectively.

The largest temperature gradient of any of the six cooling methods occurs in the case of film cooling with no convection (ADFC). Also, the average wall temperature for this case is high are not appreciably different than that for CONV cooling. However, combining both convection and film cooling results in a considerable reduction in wall temperature, as seen from the CFFC and PFFC temperature profiles. As expected, the counterflow results indicate a lower temperature gradient than PFFC through the aver-

age surface temperature is approximately the same for the two cooling methods. The surface temperatures for CFFC are higher than for TRANS but less than for FCFC.

Examination of equations (17) and (28) indicates that the relative order of the average surface temperature for CFFC, TRANS, and FCFC is due primarily to the respective magnitudes of η_{film}. The larger η_{film} is, the smaller the coefficients are of both the $T_{c,2}$ and T_{ge} terms in these equations. The film protection provided by injection through holes (FCFC) is much less than that available with continuous slot injection. This fact is clearly illustrated by the η_{film} values (given in the insert) for each of the cooling schemes.

Large surface-temperature variation for CFFC. - Counterflow film cooling can result in large surface-temperature variations, as seen in figure 7. The question arises as to whether CFFC continues to compare favorably with the other five cooling methods when L departs from the length associated with the minimum surface-temperature variation. Similar to figures 12(a) and (b), figures 12(c) and (d) compare the six cooling schemes but with L equal to 25 and 2.5 centimeters for pressures of 5 and 40 atmospheres, respectively. These values of L are lengths which result in the largest surface-temperature differences for CFFC, as shown in figure 7. Though the CFFC surface-temperature differences are large (327 and 300 K (588° and 540° F) for gas pressures of 5 and 40 atm, respectively), the surface-temperature variation for PFFC is larger. Because of the rapidly decaying film layer, the ADFC results again indicate the largest wall-temperature rise. The low convection effectiveness for the short section (fig. 12(d)) causes the high surface temperatures for the CONV scheme. The large reduction in surface temperature for FCFC and TRANS between figures 12(b) and (d) at 40 atmospheres pressure is due to the large increase in the quantity of cooling air required to cool the short CFFC sections at high pressure. This result is demonstrated more clearly in the next section. The only effect that the axial length of the cooled wall has on FCFC and TRANS is that the average heat-transfer coefficient over the surface increases as L decreases.

From the interpretation of results presented in figure 12, it is evident that the most efficient use of cooling air is achieved when film and convection cooling are combined. It is also apparent that CFFC combines these two modes of heat transfer in a complementary manner to yield significantly smaller surface-temperature variations than PFFC. In fact, for the conditions studied herein, CFFC is competitive with TRANS and FCFC.

Comparison of TRANS, FCFC, and CFFC on the Basis of Coolant Flow Rate

Given in figure 13 as a function of gas pressure is the ratio of the coolant flow rate required to cool a given surface to a temperature of 1255 K (1800° F) by TRANS and FCFC to the corresponding coolant mass flux for CFFC as obtained from figure 7. In

the latter case, the maximum surface temperature is equal to 1255 K (1800° F); but the average surface temperature can be considerably lower, resulting in some conservatism toward CFFC in the comparison. The required coolant mass-flux rate increases more rapidly with pressure for CFFC than for either TRANS or FCFC, thereby explaining the decrease in the coolant flow rate ratio in figure 13. The relative difficulty in cooling the short sections by CFFC is reflected in the curves for L = 2.5 centimeters in the figure.

A comparison of the variation in convection effectiveness with pressure between the three cooling methods is helpful in explaining the coolant mass-flow rate distributions. Referring to equation (27) for TRANS and FCFC and, in a qualitative sense, to equation (18) for CFFC, it can be seen that the required mass-flux rate varies inversely with η'. Figure 14 contains the ratio of η'_{cffc} (from fig. 8) to η'_{fcfc} and η'_{trans} normalized on the 5-atmosphere-pressure case. The ratio between the cooling cases for figures 13 and 14 are reversed to more clearly illustrate the same general trends in the curves. The convection effectiveness decreases more rapidly with pressure for CFFC than for either TRANS or FCFC. Also, as was indicated in figure 8, η'_{cffc} decreases with pressure more rapidly for the shorter sections than for the longer ones.

Cumulative Effect of Slots in Series

The results presented thus far have not considered the cumulative effect caused by replenishing the film layer when a number of shorter CFFC segments are arranged in series. However, the general conclusions drawn about one segment still hold for one of a series of segments; only the film effectiveness does not decay as rapidly when there is a carryover of a residual film layer from an upstream segment.

Several factors are involved when considering whether it is more efficient to use one long section (assuming there is sufficient coolant pressure available) or a series of shorter sections. If it is assumed that the film effectiveness at a distance L from the slot is significant enough to effect the downstream section, then as the number of sections increases and their length decreases, η' decreases and η_{film} increases. These changes in η' and η_{film} can have opposite effects on the required coolant flow rate. As discussed previously, decreasing η' with a given film effectiveness increases the required coolant flow. On the other hand, increasing η_{film} can reduce G_c especially if η' is small (see eq. (18)).

As an example of the cumulative effect of multiple slots, CFFC was applied to a surface 10 centimeters in length, assuming both one full-length segment and two and three equal-length segments in series. The results are given in figure 15 for a gas pressure of 40 atmospheres. The maximum temperature for each segment was assumed to be maintained at 1255 K (1800° F). The coolant mass-flux ratio is based on the average

coolant mass velocity over the 10-centimeter-length surface area. Recall from the analysis in the subsection entitled Summation of film effectiveness for multiple slots that these results are optimistic because an upper bound was assumed for the cumulative film effectiveness. The temperature gradients increase and the pressure drop decreases as the number of segments increase, while the coolant requirements remain approximately the same for all three cases.

SUMMARY OF RESULTS

The results of an analysis and comparison of various cooling schemes for walls of gas turbine engine components are summarized as follows:

1. In the high gas temperature and pressure environments expected in future gas turbine engines, convection cooling of turbine components must be augmented by film cooling. It is beneficial to utilize as much of the heat sink available in the cooling air as possible for convection cooling before ejecting it as a film. Increasing convection effectiveness reduces the cooling air required to maintain a given average wall temperature.

2. The most efficient use of cooling air is achieved when film and convection cooling are combined, as in transpiration, full-coverage, counterflow, and parallel-flow film cooling. The coolant requirements for counterflow film cooling are greater than for transpiration cooling, as expected, but can be significantly less than for full-coverage film cooling. This relative order in cooling efficiency is due primarily to the respective magnitudes of the film effectiveness associated with each cooling scheme. The film protection provided by injection through discrete holes (full-coverage film cooling) is much less than that available with continuous slot injection (counterflow film cooling).

3. Low surface-temperature variations are possible with transpiration and full-coverage film cooling because of the capability of regulating the mass injection locally with these two cooling methods. Counterflow film cooling yields much smaller surface-temperature variations over a segment length than parallel-flow and adiabatic film cooling. The latter scheme resulted in the largest surface-temperature gradients of the cooling methods analyzed.

4. A distinct minimum in the surface-temperature variation for counterflow film cooling occurs when film and convection cooling are properly balanced for a given segment.

Lewis Research Center,
National Aeronautics and Space Administration,
Cleveland, Ohio, October 12, 1971,
764-74.

APPENDIX - SYMBOLS

A	area
A_{eff}	effective area of finned surface
A_{fin}	fin area
A_p	coolant passage cross-sectional area
B	dimensionless parameter, $G_c C_{p,g}/\bar{h}_g$
b	coolant passage height
C_p	specific heat
D_H	hydraulic diameter
f	friction factor
G_c	average coolant mass-flux rate based on cooled surface area
$G_{c,p}$	average coolant mass-flux rate based on passage flow area
G_g	hot-gas mass-flux rate
h_c	coolant-side heat-transfer coefficient
$\bar{h}_g$	average gas-to-surface heat-transfer coefficient
h_{gx}	local gas-to-surface heat-transfer coefficient
j	Colburn heat-transfer factor
K'	entrance pressure loss coefficient
K''	exit pressure loss coefficient
k	thermal conductivity
L	axial length of cooled surface area
l	fin height
M	Mach number
m	slot mass-flux ratio, $(\rho V)_s/G_g$
NF	number of fins per centimeter
Nu	Nusselt number
P	total pressure
Pr	Prandtl number
p	static pressure

Q	heat-transfer rate
q	heat-flux rate
R	gas constant
Re	Reynolds number
s	slot height
T	temperature
T_c	total coolant temperature
T_g	total gas temperature
T_{ge}	effective gas temperature (or recovery temperature)
T_{ref}	reference gas temperature
T_w	wall temperature
t	wall thickness
t_g	static gas temperature
V	velocity
x	spacial coordinate in axial direction
x_o	boundary-layer development length
γ	specific heat-ratio
δ	fin thickness
η_{film}	film effectiveness, $\frac{T_{ge} - T_{aw}}{T_{ge} - T_{c,2}}$
$\bar{\eta}_{film}$	average film effectiveness, $\frac{T_{ge} - (T_{aw})_{avg}}{T_{ge} - T_{c,2}}$
η_{fin}	fin effectiveness
η'	convection effectiveness
η'_{cffc}	CFFC convection effectiveness, $\frac{T_{c,2} - T_{c,i}}{(T_{w,2})_{max} - T_{c,i}}$
η'_{conv}	CONV convection effectiveness, $\frac{T_{c,2} - T_{c,i}}{(T_{w,2})_{max} - T_{c,i}}$

η'_{fcfc} FCFC convection effectiveness, $\dfrac{T_{c,2} - T_{c,i}}{T_{w,2} - T_{c,i}}$

η'_{o} reference convection effectiveness

η'_{pffc} PFFC convection effectiveness, $\dfrac{T_{c,2} - T_{c,i}}{(T_{w,2})_{max} - T_{c,i}}$

η'_{trans} TRANS convection effectiveness, $\dfrac{T_{c,2} - T_{c,i}}{T_{w,2} - T_{c,i}}$

μ viscosity

ρ density

φ temperature-difference ratio, $\dfrac{T_{ge} - T_{w,2}}{T_{ge} - T_{c,i}}$

$\overline{\varphi}$ average temperature-difference ratio, $\dfrac{T_{ge} - (T_{w,2})_{avg}}{T_{ge} - T_{c,i}}$

φ_{min} minimum temperature-difference ratio, $\dfrac{T_{ge} - (T_{w,2})_{max}}{T_{ge} - T_{c,i}}$

ξ dimensionless distance, x/L

Subscripts:

adfc adiabatic film cooling

avg average

aw adiabatic wall with film cooling

c coolant

cffc counterflow film cooling

conv convection cooling

fcfc full-coverage film cooling

g gas

i coolant supply condition

max maximum

min minimum

opf	offset plate fin
pffc	parallel-flow film cooling
ref	reference
s	slot
trans	transpiration cooling
uf	unfinned
w	wall
1	location at interface between coolant and wall
2	location at interface between hot gas and wall
(i)	coolant passage station (i = 1, 2, 3, . . .)

REFERENCES

1. Esgar, Jack B.; Colladay, Raymond S.; and Kaufman, Albert: An Analysis of the Capabilities and Limitations of Turbine Air Cooling Methods. NASA TN D-5992, 1970.

2. Livingood, John N. B.; Ellerbrock, Herman H.; and Kaufman, Albert: 1971 NASA Turbine Cooling Research Status Report. NASA TM X-2384, 1971.

3. Goldstein, R. J.; Eckert, E. R. G.; and Ramsey, J. W.: Film Cooling with Injection Through a Circular Hole. Rep. HTL-TR-82, Univ. of Minnesota. (NASA CR-54604), May 14, 1968.

4. Kays, William M.: Convective Heat and Mass Transfer. McGraw-Hill Book Co., Inc., 1966.

5. Eckert, E. R. G.; and Drake, Robert M., Jr.: Heat and Mass Transfer. Second ed., McGraw-Hill Book Co., Inc., 1959.

6. Poferl, David J.; Svehla, Roger A.; and Lewandowski, Kenneth: Thermodynamic and Transport Properties of Air and the Combustion Products of Natural Gas and of ASTM-A1 Fuel with Air. NASA TN D-5452, 1969.

7. London, A. L.; and Shah, R. K.: Offset Rectangular Plate-Fin Surface - Heat Transfer and Flow Friction Characteristics. J. Eng. Power, vol. 90, no. 3, July 1968, pp. 218-228.

8. Hartnett, J. P.; Birkebak, R. C.; and Eckert, E. R. G.: Velocity Distributions, Temperature Distributions, Effectiveness and Heat Transfer for Air Injected Through a Tangential Slot Into a Turbulent Boundary Layer. J. Heat Transfer, vol. 83, no. 3, Aug. 1961, pp. 293-306.

9. Burggraf, F.; Murtaugh, J. P.; and Wilton, M. E.: Design and Analysis of Cooled Turbine Blades. Part III - Transpiration and Multiple Samll Hole Film Cooled Nozzles and Buckets. Rep. R68AEG103, General Electric Co. (NASA CR-54515), Jan. 1, 1968.

10. Moffat, R. J.; and Kays, W. M.: The Turbulent Boundary Layer on a Porous Plate: Experimental Heat Transfer with Uniform Blowing and Suction. Rep. HMT-1, Stanford Univ., 1967.

11. Simpson, R. L.; Kays, W. M.; and Moffat, R. J.: The Turbulent Boundary Layer on a Porous Plate: Experimental Study of the Fluid Dynamics with Injection and Suction. Rep. HMT-2, Stanford Univ., 1967.

12. Whittan, D. G.; Kays, W. M.; and Moffat, R. J.: The Turbulent Boundary Layer on a Porous Plate: Experimental Heat Transfer with Variable Suction, Blowing, and Surface Temperature. Rep. HMT-3, Stanford Univ., 1967.

13. Julien, H. L.; Kays, W. M.; and Moffat, R. J.: The Turbulent Boundary Layer on a Porous Plate: An Experimental Study of the Effects of a Favorable Pressure Gradient. Rep. HMT-4, Stanford Univ. (NASA CR-104140), 1969.

14. Thielbahr, W. H.; Kays, W. M.; and Moffat, R. J.: The Turbulent Boundary Layer on a Porous Plate: Experimental Heat Transfer with Blowing, Suction, and Favorable Pressure Gradient. Rep. HMT-5, Stanford Univ. (NASA CR-104141), 1969.

15. Spalding, D. B.: A Standard Formulation of the Steady Convective Mass Transfer Problem. Int. J. Heat Mass Transfer, vol. 1, no. 2/3, 1960, pp. 192-207.

16. Mickley, H. A.; Ross, R. C.; Squyers, A. L.; and Stewart, W. E.: Heat, Mass, and Momentum Transfer for Flow Over a Flat Plate with Blowing or Suction. NACA TN 3208, 1954.

17. Nealy, David A.; and Anderson, R. Daryel: Heat Transfer Characteristics of Laminated Porous Materials. Rep. EDR-5856, General Motors Corp. (AFAPL-TR-68-98, AD-391895), Aug. 1968.

18. Anderson, R. D.; Davis, W. C.; McLoed, R. N.; and Nealy, D. A.: High Temperature Cooled Turbine Blades. Rep. EDR-6176, General Motors Corp. (AFAPL-TR-69-41, AD-504209L), May 1969.

19. Goldstein, R. J.; Eckert, E. R. G.; Eriksen, V. L.; and Ramsey, J. W.: Film Cooling Following Injection Through Inclined Circular Tubes. Rep. HTL-TR-91, Univ. of Minnesota. (NASA CR-72612), Nov. 1969.

20. Ramsey, J. W.; and Goldstein, R. J.: Interaction of a Heated Jet with a Deflecting Stream. Rep. HTL-TR-92, Univ. of Minnesota. (NASA CR-72613), Apr. 1970.

21. Colladay, Raymond S.; and Stepka, Francis S.: Examination of Boundary Conditions for Heat Transfer Through a Porous Wall. NASA TN D-6405, 1971.

22. Bayley, F. J.; and Turner, A. B.: The Transpiration-Cooled Gas Turbine. Paper 70-GT-56, ASME, May 1970.

23. Shapiro, Ascher H.: The Dynamics and Thermodynamics of Compressible Fluid Flow. Ronald Press Co., 1953.

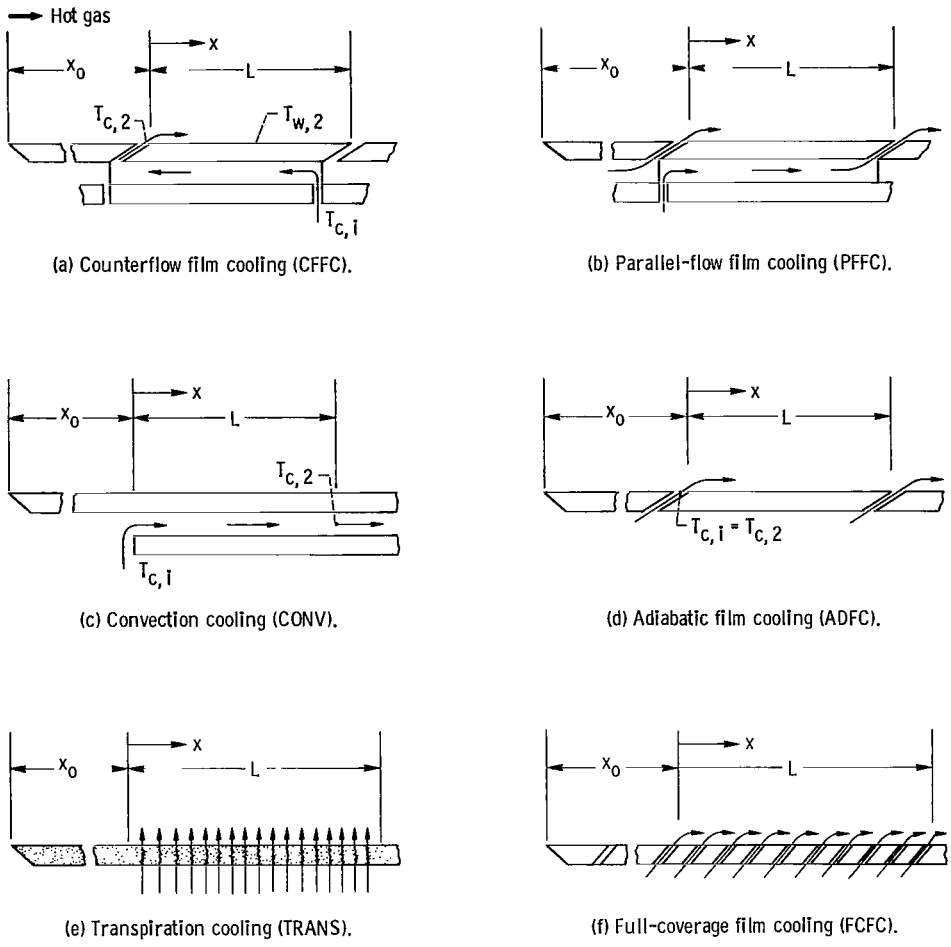

(a) Counterflow film cooling (CFFC).

(b) Parallel-flow film cooling (PFFC).

(c) Convection cooling (CONV).

(d) Adiabatic film cooling (ADFC).

(e) Transpiration cooling (TRANS).

(f) Full-coverage film cooling (FCFC).

Figure 1. - Heat-transfer models.

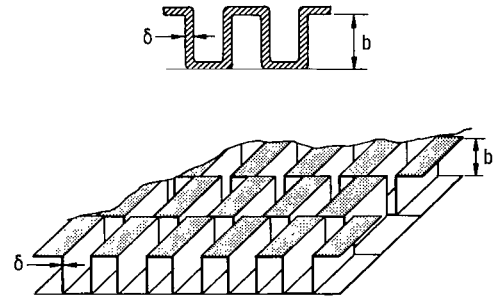

Figure 2. - Offset rectangular plate fin configuration.

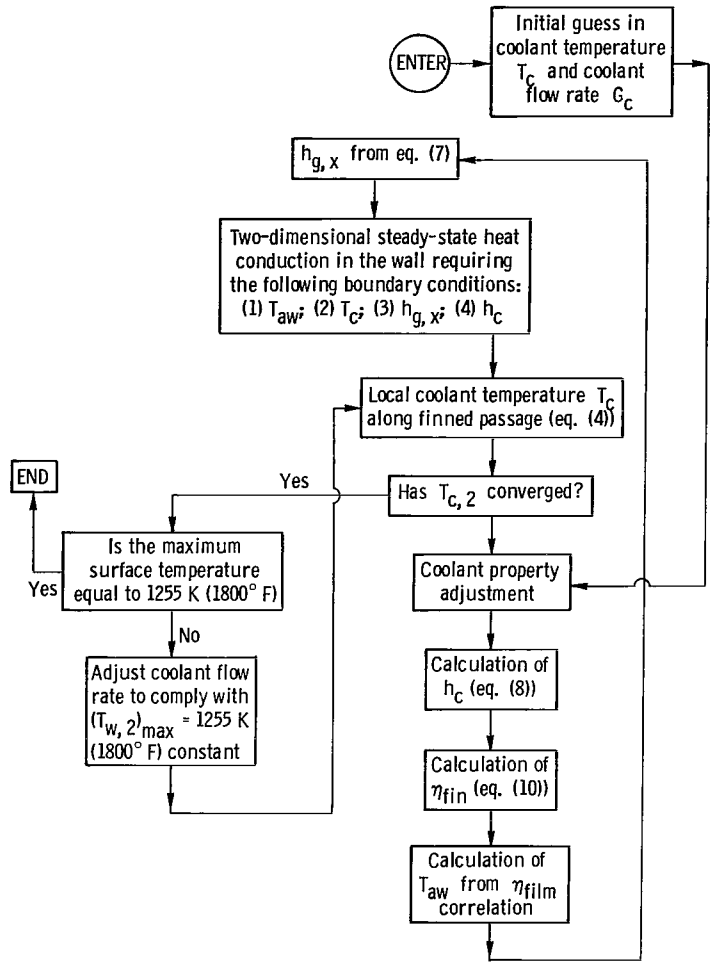

Figure 3. - Flow chart describing program logic.

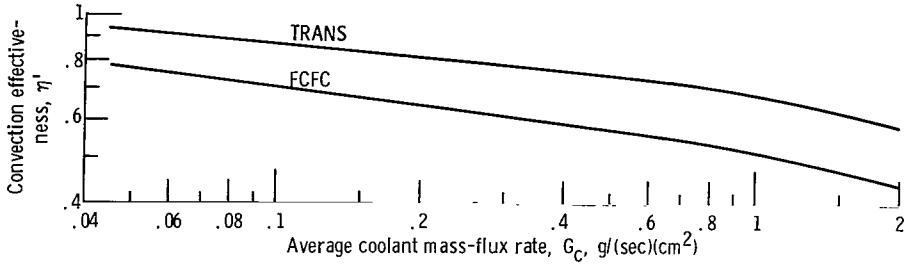

Figure 4. - Convection effectiveness distribution for transpiration-cooled (TRANS) and full-coverage-film-cooled (FCFC) walls. Effective thermal conductivity, 13.8 J/(sec)(m)(K); wall thickness, 0.0114 centimeter.

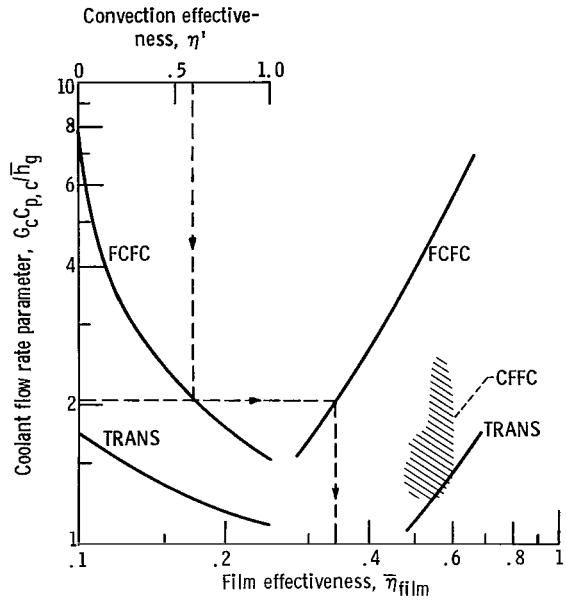

Figure 5. - Interaction of convection and film cooling. Effective gas temperature, 2200 K (3500° F); maximum outer wall temperature, 1255 K (1800° F); coolant supply temperature, 811 K (1000° F). TRANS, transpiration cooling; FCFC, full-coverage film cooling; CFFC, counterflow film cooling.

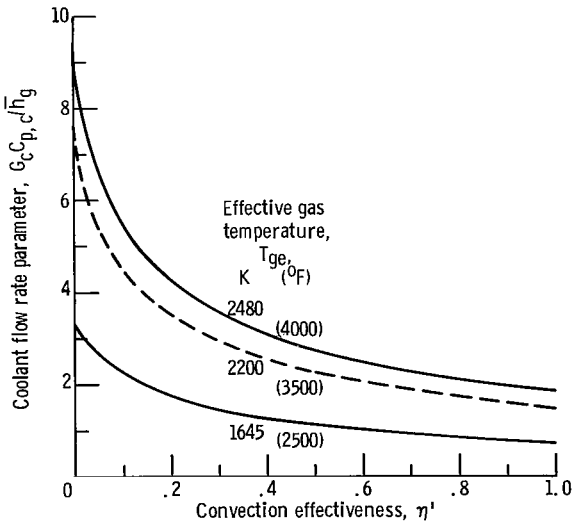

Figure 6. - Effect of convection on coolant requirements for full-coverage film-cooled wall. Outer wall temperature, 1255 K (1800° F); coolant supply temperature, 811 K (1000° F).

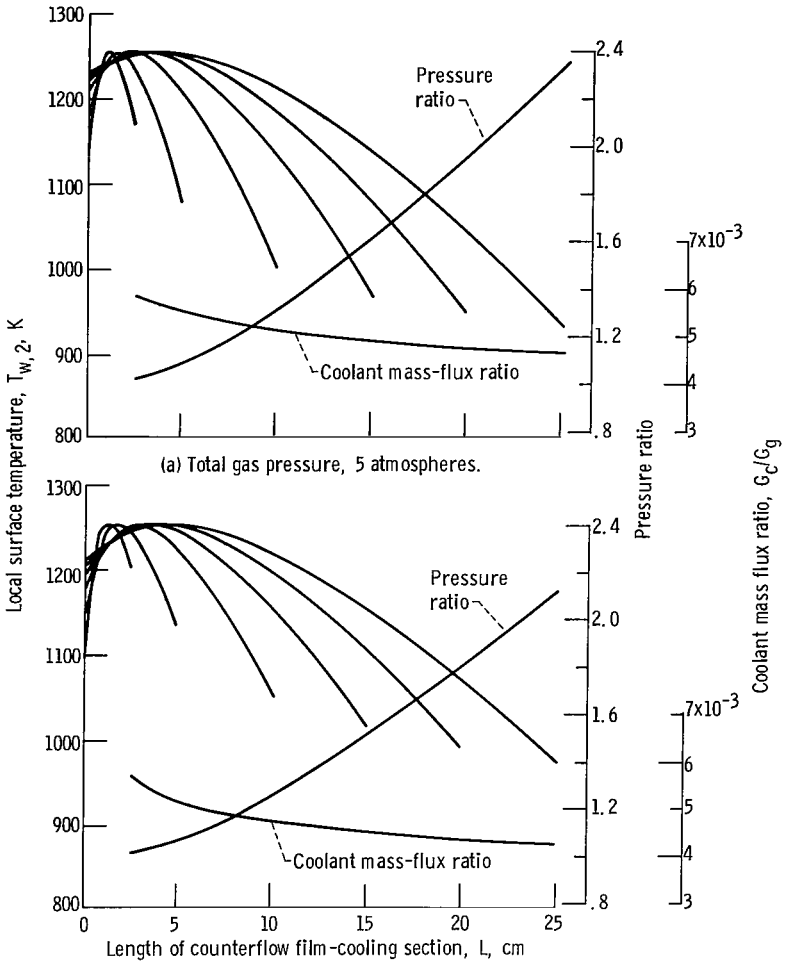

(a) Total gas pressure, 5 atmospheres.

(b) Total gas pressure, 10 atmospheres.

Figure 7. - Counterflow film-cooled wall section. Offset-plate-finned cooling passage; effective gas temperature, 2200 K (3500° F); coolant supply temperature, 811 K (1000° F).

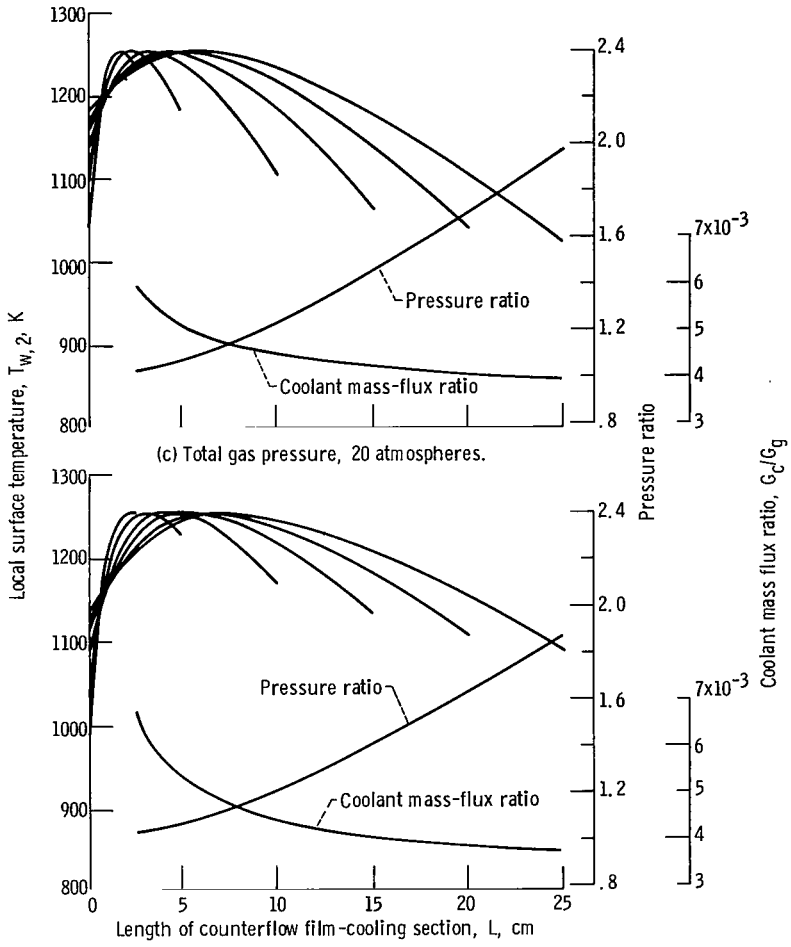

(c) Total gas pressure, 20 atmospheres.

(d) Total gas pressure, 40 atmospheres.

Figure 7. - Concluded.

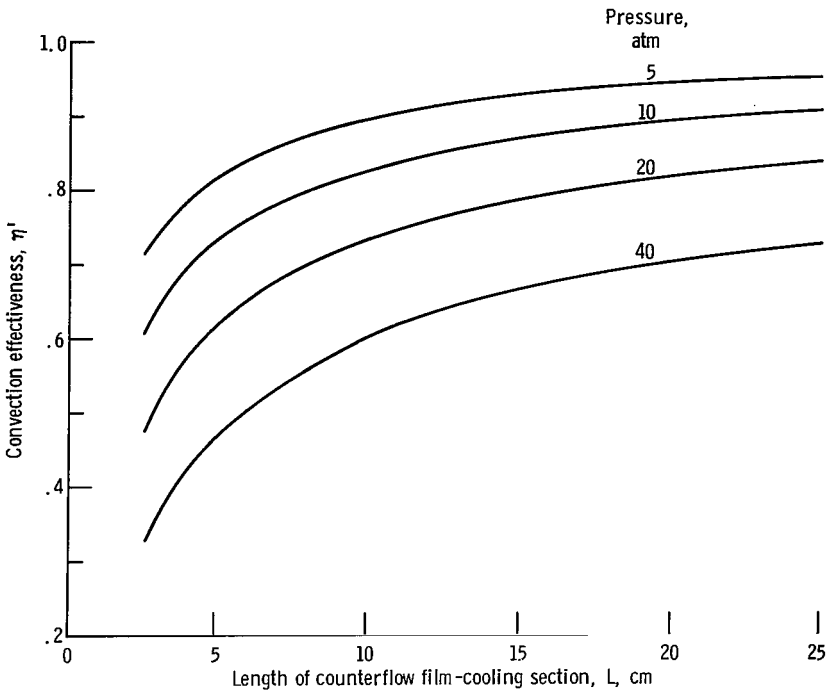

Figure 8. - Effect of section length and gas pressure on convection effectiveness for counterflow film cooling. Maximum outer wall temperature, 1255 K (1800° F); effective gas temperature, 2200 K (3500° F); coolant supply temperature, 811 K (1000° F).

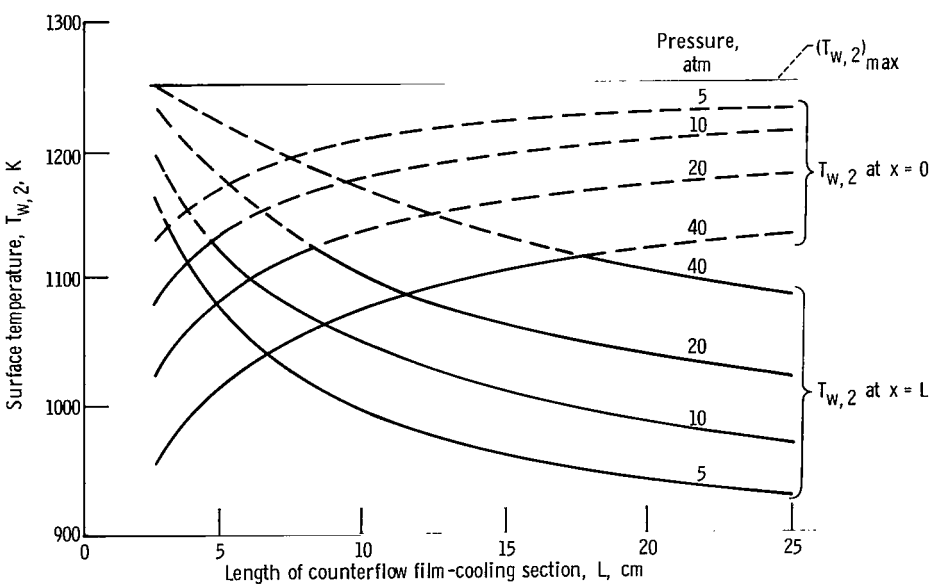

Figure 9. - Hot-gas-side surface temperatures at each end of counterflow film-cooling segment.

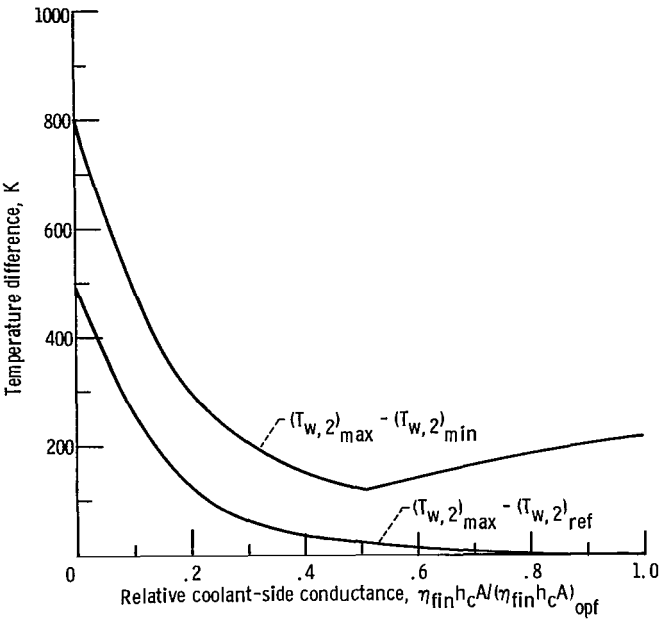

Figure 10. - Effect of overall coolant-side conductance on surface temperatures for counterflow film cooling. Constant coolant flow rate; reference outer wall temperature, $(T_{w,2})_{ref}$, 1255 K (1800° F); total gas pressure, 5 atmospheres; segment length, 7.5 cm; effective gas temperature, 2200 K (3500° F); coolant supply temperature, 811 K (1000° F).

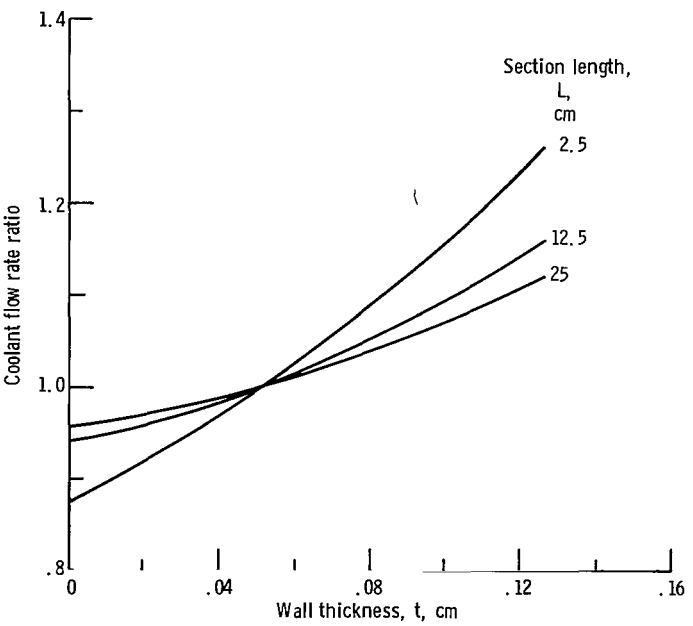

Figure 11. - Effect of wall thickness on coolant requirements for counterflow film cooling. Maximum outer wall temperature, 1255 K (1800° F); total gas pressure, 40 atmospheres; effective gas temperature, 2200 K (3500° F); coolant supply temperature, 811 K (1000° F).

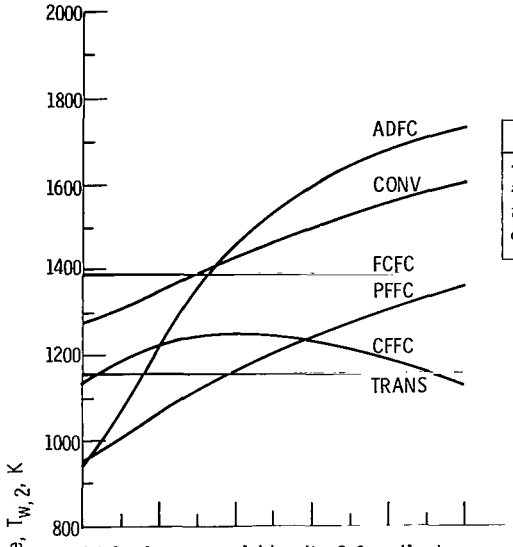

	TRANS	FCFC	CFFC	PFFC	CONV	ADFC
η'	0.80	0.64	0.74	0.65	0.73	----
$\overline{\eta}_{film}$	.58	.27	.57	.57	----	0.57
$\overline{\varphi}$	.75	.58	.71	.72	.53	.53
φ_{min}	.75	.58	.68	.60	.43	.34

(a) Surface area axial length, 3.0 centimeters; total gas pressure, 5 atmospheres.

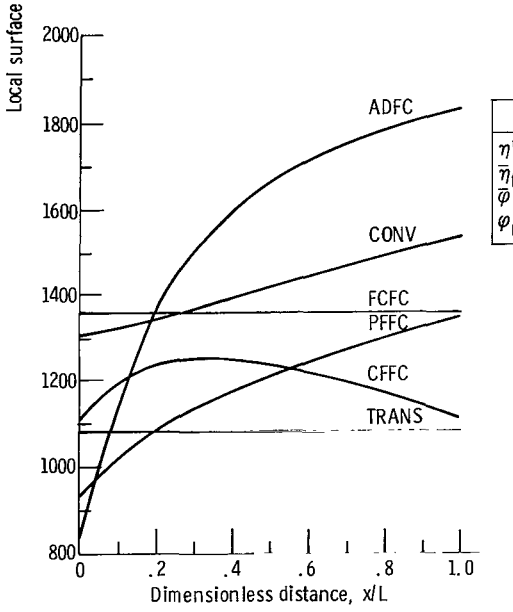

	TRANS	FCFC	CFFC	PFFC	CONV	ADFC
η'	0.65	0.50	0.69	0.60	0.76	----
$\overline{\eta}_{film}$	.67	.31	.49	.49	----	0.49
$\overline{\varphi}$	.80	.60	.71	.72	.56	.45
φ_{min}	.80	.60	.68	.61	.47	.26

(b) Surface area axial length, 17.7 centimeters; total gas pressure, 40 atmospheres.

Figure 12. - Surface-temperature distribution for various cooling schemes, based on the same coolant mass-flux ratio for a given surface area. Effective gas temperature, 2200 K (3500° F); coolant supply temperature, 811 K (1000° F).

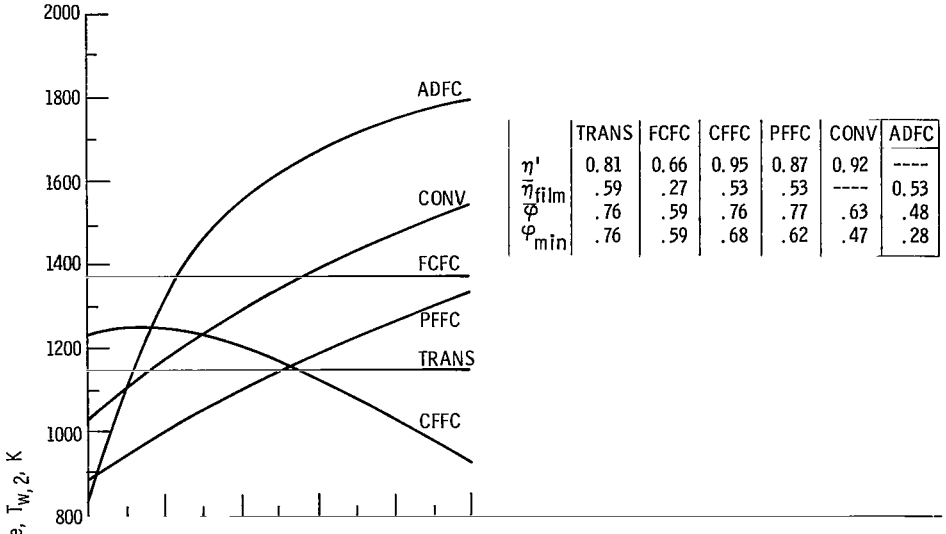

	TRANS	FCFC	CFFC	PFFC	CONV	ADFC
η'	0.81	0.66	0.95	0.87	0.92	----
$\bar{\eta}_{film}$	.59	.27	.53	.53	----	0.53
$\bar{\varphi}$	.76	.59	.76	.77	.63	.48
φ_{min}	.76	.59	.68	.62	.47	.28

(c) Surface area axial length, 25 centimeters; total gas pressure, 5 atmospheres.

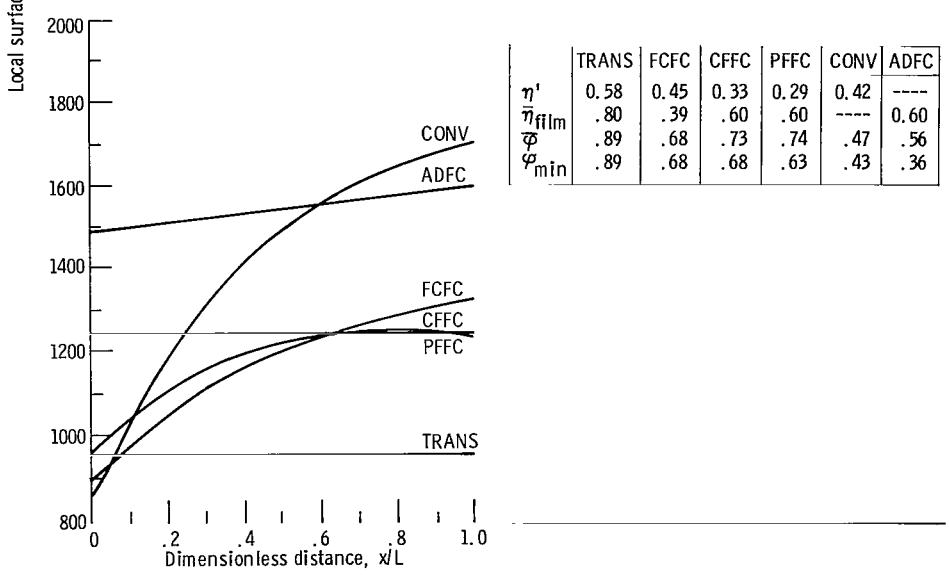

	TRANS	FCFC	CFFC	PFFC	CONV	ADFC
η'	0.58	0.45	0.33	0.29	0.42	----
$\bar{\eta}_{film}$	.80	.39	.60	.60	----	0.60
$\bar{\varphi}$	.89	.68	.73	.74	.47	.56
φ_{min}	.89	.68	.68	.63	.43	.36

(d) Surface area axial length, 2.5 centimeters; total gas pressure, 40 atmospheres.

Figure 12. - Concluded.

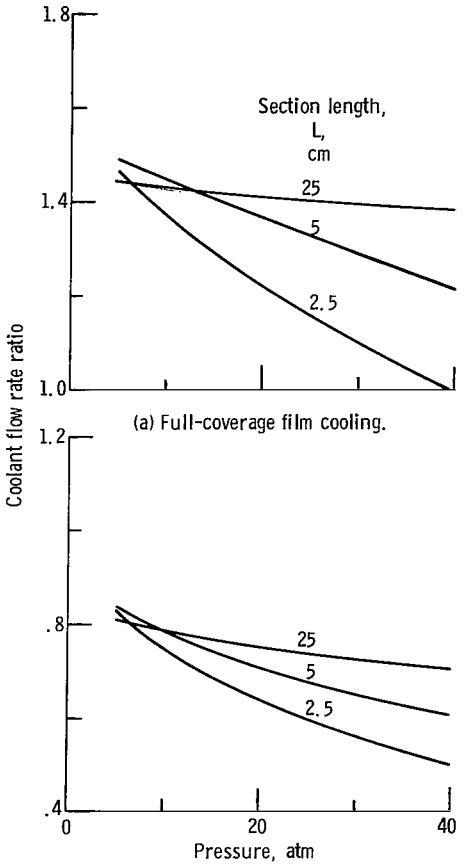

(a) Full-coverage film cooling.

(b) Transpiration cooling.

Figure 13. - Effect of pressure on coolant requirements of transpiration cooling and full-coverage film cooling relative to counterflow film cooling. Maximum outer wall temperature, 1255 K (1800° F).

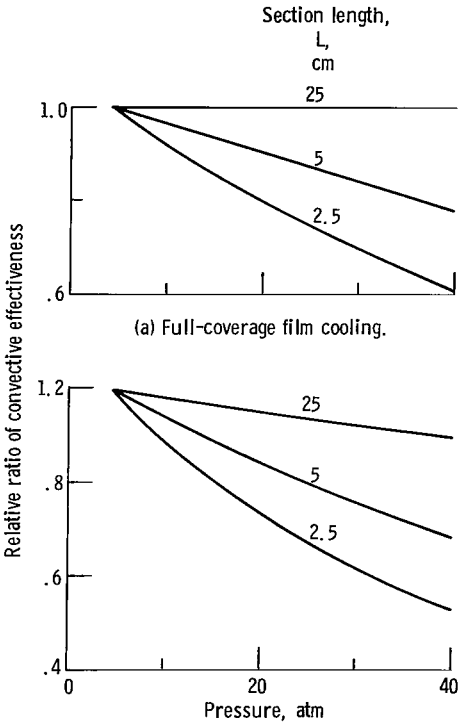

(a) Full-coverage film cooling.

(b) Transpiration cooling.

Figure 14. - Effect of pressure on variation of convection effectiveness for counterflow film cooling relative to transpiration cooling and full-coverage film cooling. Maximum outer wall temperature, 1255 K (1800° F).

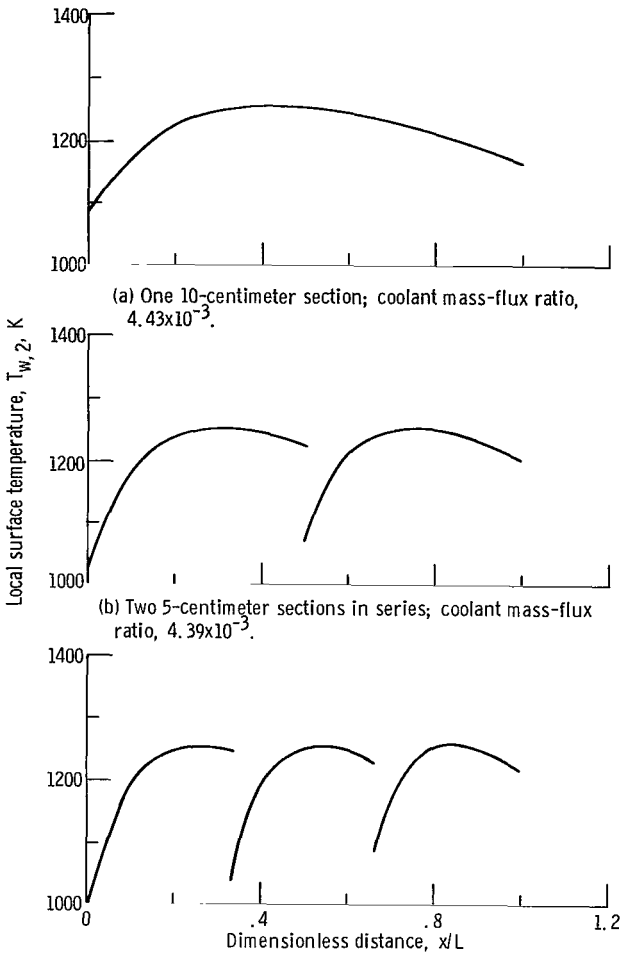

(a) One 10-centimeter section; coolant mass-flux ratio, 4.43×10^{-3}.

(b) Two 5-centimeter sections in series; coolant mass-flux ratio, 4.39×10^{-3}.

(c) Three 3.3-centimeter sections in series; coolant mass-flux ratio, 4.34×10^{-3}.

Figure 15. - Cumulative film effect from multiple slots with counterflow film-cooling scheme. Axial surface area length, 10 centimeters; effective gas temperature, 2200 K (3500^{0} F); total gas pressure, 40 atmospheres.

"The aeronautical and space activities of the United States shall be conducted so as to contribute . . . to the expansion of human knowledge of phenomena in the atmosphere and space. The Administration shall provide for the widest practicable and appropriate dissemination of information concerning its activities and the results thereof."

—NATIONAL AERONAUTICS AND SPACE ACT OF 1958

NASA SCIENTIFIC AND TECHNICAL PUBLICATIONS

TECHNICAL REPORTS: Scientific and technical information considered important, complete, and a lasting contribution to existing knowledge.

TECHNICAL NOTES: Information less broad in scope but nevertheless of importance as a contribution to existing knowledge.

TECHNICAL MEMORANDUMS: Information receiving limited distribution because of preliminary data, security classification, or other reasons.

CONTRACTOR REPORTS: Scientific and technical information generated under a NASA contract or grant and considered an important contribution to existing knowledge.

TECHNICAL TRANSLATIONS: Information published in a foreign language considered to merit NASA distribution in English.

SPECIAL PUBLICATIONS: Information derived from or of value to NASA activities. Publications include conference proceedings, monographs, data compilations, handbooks, sourcebooks, and special bibliographies.

TECHNOLOGY UTILIZATION PUBLICATIONS: Information on technology used by NASA that may be of particular interest in commercial and other non-aerospace applications. Publications include Tech Briefs, Technology Utilization Reports and Technology Surveys.

Details on the availability of these publications may be obtained from:

SCIENTIFIC AND TECHNICAL INFORMATION OFFICE

NATIONAL AERONAUTICS AND SPACE ADMINISTRATION

Washington, D.C. 20546